Chemical Engineering Journal 494 (2024) 153152

Contents lists available at ScienceDirect

Chemical Engineering Journal

journal homepage: www.elsevier.com/locate/cej

Erythrocyte membrane-camouflaged nanodelivery strategy enhances gene editing efficiency of Cas9 RNP for boosting tumor senescence

Silin Shi [a,1], Chao Chen [a,1,*], Xueting Shen [a,1], Shiyu Du [b], Kunguo Liu [a], Yamei Gao [c], Lihua Qu [d], Jingjing Yang [a], Mengfan Tang [a,*], Xin Han [a,*]

[a] The Second Affiliated Hospital of Nanjing University of Chinese Medicine, Jiangsu Collaborative Innovation Center of Chinese Medicinal Resources Industrialization, School of Medicine, Nanjing University of Chinese Medicine, Nanjing 210023, China
[b] College of Engineering and Applied Sciences, Nanjing University, Nanjing 210023, China
[c] Department of Dermatology, First Affiliated Hospital of Nanjing Medical University and Jiangsu Province People's Hospital, Nanjing 210029, China
[d] School of Basic Medical Sciences, Xianning Medical College, Hubei University of Science and Technology, Hubei 437000, China

ARTICLE INFO

Keywords:
Erythrocyte membrane
CRISPR-Cas9 system
Azidothymidine
Telomere disorder
Tumor senescence

ABSTRACT

CRISPR-Cas9 system has emerged as an effective tool for sequence-specific gene knockout through non-homologous end joining (NHEJ). However, the inefficient precise editing of genome sequences remains a challenge for clinical treatment. Herein, an erythrocyte membrane (EM)-camouflaged and tumor microenvironment (TME)-responsive nanosystem was constructed to achieve synergistic combination of enhanced Cas9 ribonucleoprotein (RNP) gene editing efficiency and telomere dysfunction, and thus precise induced tumor inhibition. The EM-camouflaged nanosystem escaped from the reticuloendothelial system (RES) and was endocytosed by tumor cells. Azidothymidine (AZT) was gradually released as the erythrocyte shell ablation, which competitively prevented the binding of single nucleotides to the telomere replication template TR, terminate the extension of the telomerase DNA chain. Additionally, Cas9 RNP was released through disulfide bond cleavage and entered into the nucleus to realize genome editing of telomerase reverse transcriptase (TERT) gene. Simultaneous, AZT enhanced NHEJ pathway to improve the gene editing efficiency of Cas9 RNP, which further promoted the progressive telomere erosion and thus induced tumor inhibition. Overall, this biomembrane-camouflaged nanosystem realizes enhanced Cas9 RNP gene editing efficiency with high-level biosafety and promotes tumor senescence by triggering telomere disorder, which provides strategy for improving the gene editing efficiency to induce senescence of tumor cells.

1. Introduction

Genome editing is a potential technology that introduces DNA mutations into the target sequence in the form of insertions, deletions (indels), and base substitutions, which provides a powerful tool for improving biology through the precise editing of cellular DNA sequences [1]. Gene therapy (GT) is a promising therapeutic strategy to address the process of carcinogenesis by altering gene expression [2]. Clustered regularly interspaced short palindromic repeat-associated protein 9 (CRISPR-Cas9) technology has been widely used in GT because of its simplicity, versatility, high specificity and efficiency [3,4]. CRISPR-Cas9 has become an effective tool for sequence-specific gene knockout through non-homologous end joining (NHEJ) and homology-directed repair (HDR) [5]. Specifically, Cas9 nuclease cleaves the target sequences of gene and induces DNA double-stranded break (DSB), and the broken DNA is repaired using the NHEJ pathway, in which mismatch events such as base insertions or deletions occur, leading to frameshift mutations and ultimately gene inactivation [6]. In terms of the CRISPR-Cas9 forms for delivery, compared to the forms of plasmid DNA and mRNA, Cas9 ribonucleoprotein (RNP) has the advantages of low off-target, low cytotoxicity and high editing efficiency [7]. In recent years, CRISPR-Cas9 technology have been used to treat multiple diseases, including cancers, due to its excellent precision gene editing capacity [8,9]. However, CRISPR-Cas9 technology still faces some challenges in the treatment of solid tumors, including low editing efficiency [10] and low delivery efficiency [11].

* Corresponding authors.
E-mail addresses: cchen22@njucm.edu.cn (C. Chen), mengfantang@njucm.edu.cn (M. Tang), xhan0220@njucm.edu.cn (X. Han).
[1] These authors contributed equally.

https://doi.org/10.1016/j.cej.2024.153152
Received 25 April 2024; Received in revised form 4 June 2024; Accepted 14 June 2024
Available online 16 June 2024

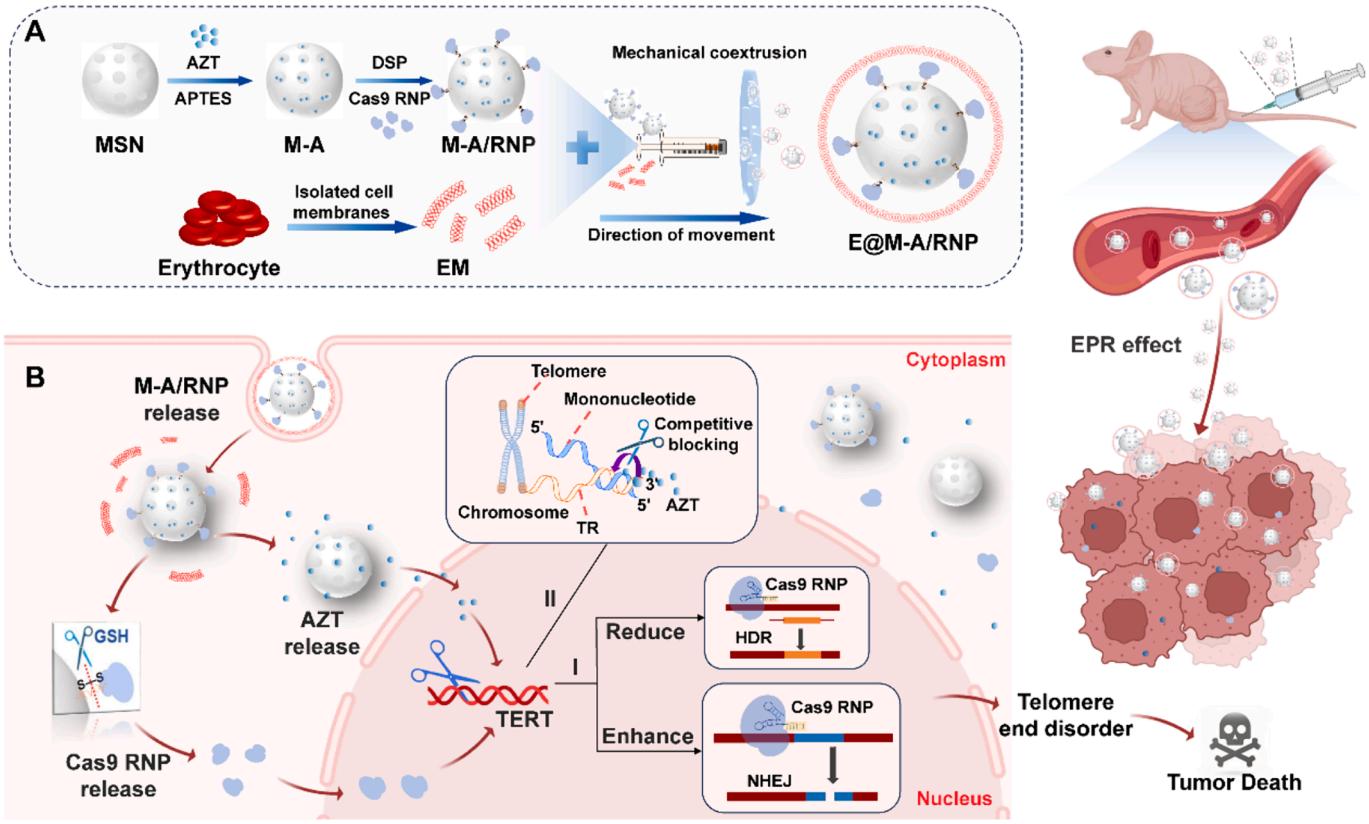

Scheme 1. Schematic illustration of enhancing Cas9 RNP gene editing efficiency in anti-tumor therapy using erythrocyte membrane-camouflaged nanoparticles. A) Design and preparation of the E@M−A/RNP nanoparticles. B) The E@M−A/RNP nanoparticles induced tumor death by precision delivering AZT and Cas9 RNP to enhance telomere end disorder. Firstly, E@M−A/RNP was injected intravenously and aggregated at the tumor site through the EPR effects. Subsequently, E@M−A/RNP was internalized into tumor cells and released AZT and Cas9 RNP within the high GSH of TME. (I) Cas9 RNP entered into the nucleus for gene editing of TERT gene, and AZT simultaneous increased gene editing efficacy of Cas9 RNP by enhancing NHEJ and reducing HDR. In addition, (II) AZT also competitively prevented the binding of single nucleotides to the telomere replication template TR, which terminated the elongation of telomerase DNA strands. Overall, this nanosystem could enhanced Cas9 RNP gene editing efficiency and thus caused disruption of telomere terminals, ultimately leading to tumor cell death.

Telomeres are shortened due to terminal replication problems during each cell division, which gradually leads to replicative senescence [12]. Mammalian telomere length is mainly regulated by telomerase, and telomerase is a ribonucleoprotein composed of reverse transcriptase (TERT) and RNA subunit (TERC) [13]. TERC is constitutively expressed in all cells [14], whereas TERT is only expressed in 80 %-90 % of tumor cells. Tumor cells prevent progressive telomere erosion by activating the mechanism of TERT, thereby achieving proliferation and immortality. However, TERT was inactivated in somatic cells and no telomerase activity was detected [15]. To date, knocking out TERT gene using CRISPR-Cas9 system has been reported to inactivate telomerase, which may be a promising tumor treatment strategy [16]. In recent years, several methods have been developed and applied to improve the gene editing efficiency of CRISPR-Cas9 technology. For example, Richardson *et al.* found that a short segment of DNA that does not match the DNA sequence in the genome can interfere with the DNA repair mechanisms in human cells, thereby increasing the efficiency of gene editing by 2.5 to 5 times [17]. Several small molecule compounds have been studied that can effectively activate or block DNA repair pathways, such as, NHEJ or HDR [18], and can fine-tune the activity of nucleases according to dose and time [19,20]. Zhang *et al.* found farrerol, a small molecule compound, could significantly promoted HDR and thus improved the gene targeting integration efficiency of CRISPR-Cas9 system [21]. A nucleoside reverse transcriptase inhibitor, azidothymidine (AZT) has been reported that enhance the gene editing frequency of CRISPR-Cas9 system through reducing HDR and enhancing NHEJ efficiency [22]. Furthermore, AZT competitively prevents the binding of single nucleotides to the telomere replication template TR, terminating the extension of telomerase DNA chain and rendering tumor cells lose the ability to maintain effective telomere length, ultimately leading to tumor cell senescence and apoptosis [23]. Nevertheless, it is still challenging to effectively co-delivery of AZT and CRISPR-Cas9 system for synergistic combination therapy.

Although viral vectors have been widely used in the delivery of drugs or CRISPR-Cas9 system, but its uncontrolled chromosomal integration may lead to carcinogenesis and immunogenicity, which hinders its clinical application [24,25]. Non-viral nanoparticles have shown great potential for precise delivering drugs and CRISPR-Cas9 system in tumor therapy, with higher safety [26,27]. Mesoporous silica (MSN) nanoparticle has been widely used for drug delivery due to its controllable particle size, large specific surface area, modified pore size and surface chemistry, and high drug loading [28,29]. However, MSN may suffer from premature drug leakage and release during the delivery process, thus limiting efficiency of drug delivery [30]. It has been found that encapsulation of bio-membrane can optimize the defects of MSN [31]. Erythrocyte membrane (EM) has the advantages of easy to obtain, extract and modification, and nanoparticles encapsulated by EM have the advantages of good biocompatibility, anti-macrophage phagocytosis, long blood circulation time, and easy intracellular release [32,33]. Therefore, EM-coated MSN may be a potential strategy for precise delivery of AZT and CRISPR-Cas9 system.

In this study, a glutathione (GSH)-responsive EM-based biomimetic nanoplatform was established, which in combination with AZT enhanced the gene editing efficiency of Cas9 RNP for TERT gene, and induced telomere end disorder and tumor inhibition. MSN was used to load AZT (M−A) and subsequent modification of disulfide bond to

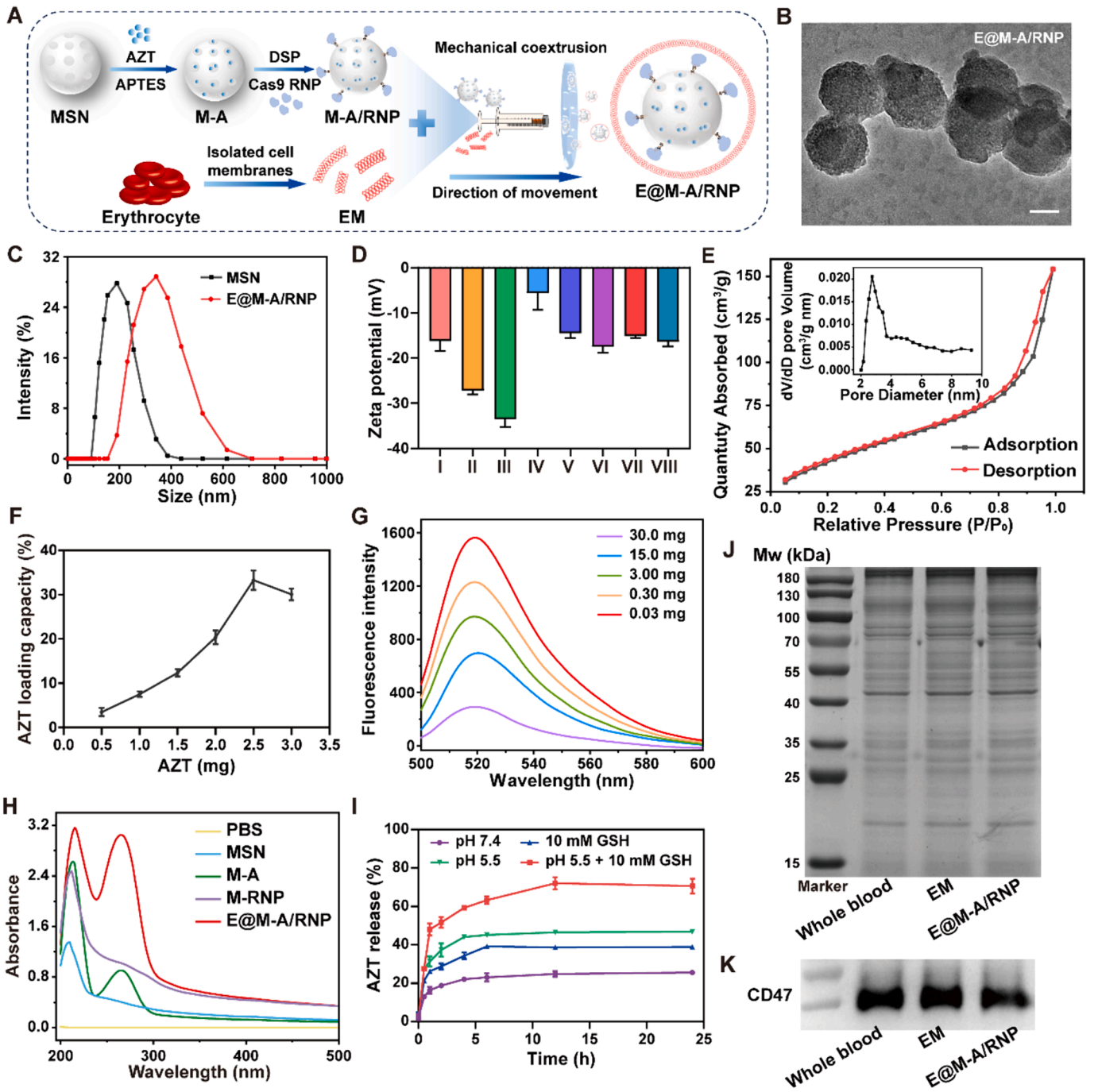

Fig. 1. Preparation and Characterization of the E@M−A/RNP nanoparticles. A) The stepwise synthesis schematic diagram of E@M−A/RNP. B) The representative transmission electron microscopy (TEM) images of E@M−A/RNP. Scale bars, 50 nm. C) Dynamic light scattering (DLS) profiles of MSN and E@M−A/RNP. D) Zeta potentials of the synthetic intermediates in the synthesis of E@M−A/RNP nanoparticles. I: MSN, II: AZT, III: M−A, IV: M−A−NH_2, V: M−A−DSP, VI: M−A/RNP, VII: EM, VIII: E@M−A/RNP. E) BET analysis and pore size distribution (inset) of MSN. F) Quantification of AZT loadings at different concentrations. G) Fluorescence spectra of supernatant after M−A−DSP (0.03, 0.3, 3.0, 15.0, 30.0 mg) incubated with FITC-labeled Cas9. H) UV–Vis–NIR absorption spectra of the synthetic intermediates. I) The AZT release from E@M−A/RNP (1 mg mL^{-1}) under different conditions. Retention of EM protein during preparation process, J) SDS-PAGE analysis whole protein and K) Western-blot analysis of CD47 protein.

connect Cas9 RNP system (M−A/RNP), and then the outermost layer encapsulated with EM to synthesize the E@M−A/RNP nanoparticle (Scheme 1**A**). The E@M−A/RNP accumulated at tumor sites due to the EPR effect and was internalized by tumor cells. The disulfide bonds were disrupted in the tumor microenvironment (TME) with a highly GSH concentration and Cas9 RNP was released and entered into the nucleus to execute gene editing of TERT gene. Meanwhile, AZT enhanced the NHEJ process to boosted the gen editing efficiency of Cas9 RNP. Furthermore, AZT competitively inhibited the binding of single nucleotides to the telomere replication template TR, hindering telomerase DNA chain extension (Scheme 1**B**). By synergistic combination of AZT and Cas9 RNP system, this biomembrane-camouflaged nanodelivery strategy realized enhanced gene editing and eventually resulted in telomere disorder, induced replicative senescence, and thus triggered tumor inhibition.

2. Materials and methods

2.1. Synthesis of the E@M−A/RNP nanoparticles

For preparation of E@M−A/RNP, AZT was firstly loaded into MSN to form M−A, and then surface modification with 3-aminopropyltriethoxysilane (APTES) and 3,3-Dithiodipropionic acid bis (N-succinimidyl ester) (DSP). The Cas9 protein and sgRNA (with a mass ratio of 1:2 between Cas9 and sgRNA) were mixed in PBS (pH = 7.4) for 5 min to form Cas9 RNP compound. The modified M−A was mixed with Cas9 RNP at 4℃ overnight and finally encapsulation of EM to obtain E@M−A/RNP nanoparticle after extrusion using a liposome extruder.

2.2. Real-time qPCR analysis of TERC level in the FLAG immunoprecipitates (IP)

The treated A549 cells with density of 8×10^6 cells were dissolved in high salt buffer on ice. The lysate was diluted with five volumes of low salt buffer and then centrifuged at 18,630 × g for 10 min at 4℃. The supernatant was collected and diluted 3–5 times with eluent. The Q-TRAP reaction system included 2 μL IP eluent, 100 ng TS primers, 100 ng ACX primers, and 1 mM EGTA were mixed in SYBR green PCR master mix. The reaction mixture was incubated at 30℃ for 30 min, and then amplified in 40 cycles using the ABI StepOnePlus real-time PCR system (Applied Biosystems) at 95℃ for 15 s and 60℃ for 60 s.

2.3. In vivo antitumor efficacy evaluation

All animal procedures were performed under the guidance of the Institutional Animal Care and Use Committee of the Nanjing University of Chinese Medicine (ethical approval number: 202309A041) and were approved by China's Committee for Research and Animal Ethics in compliance with the law for experimental animals. The collected A549 cells (5×10^6 cells) were subcutaneously injected into nude mice and mice were randomly divided into six groups when the tumor size of about 60 mm^3. For bio-distribution detection, ICG covalently modified E@M−A/RNP nanoparticles were intravenously injected into the xenograft bearing mice. After anesthetized by isoflurane, images of the mice were captured with Near-infrared optical imaging technology at the time of 0, 6, 12 and 18 h post injection, respectively. For antitumor efficacy evaluation, the A549 tumor bearing BALB/c nude mice were intravenously injected with different formulations (including PBS, E@M, E@M−RNP, E@M−A, and E@M−A/RNP with dose of 16 mg kg^{-1}) every third day for a total of seven times. The mice body weight and tumor volume were measured during the treatment process, and tumor volume was calculated by the formula: Volume (mm^3) = 0.5 × Length × $Width^2$. The mice were sacrificed at the end of the experiment, and the tumors and viscera were resected. After fixation in 4 % paraformaldehyde, the tissues were prepared into paraffin sections and then stained with H&E, TERT, and Ki67 antibodies and TUNEL.

2.4. Statistical analysis

The data are presented as the mean ± standard deviation (SD) from three different experiments. Two-tailed *t*-test ($^*P < 0.05$; $^{**}P < 0.01$; $^{***}P < 0.001$) was applied to analyze significant differences between groups.

3. Results and discussion

3.1. Preparation of the E@M−A/RNP nanoparticles

Enhancing the gene editing efficiency of CRISPR-Cas9 system may be achieved through Cas9 protein recognition and cleavage of complementary gene loci with gRNA, which activate gene repair pathways (NHEJ and HDR) and ultimately lead to gene mutations and loss of original function [34,35]. It has been reported that AZT can act on the NHEJ pathway and greatly improve the gene editing efficiency [36]. Therefore, the gene editing enhancement effect of AZT was validated on CRISPR-Cas9 system, and A549-eGFP cells were selected as subjects. After transfection of CRISPR-Cas9 plasmid for eGFP gene editing into A549-eGFP cells, more green fluorescence was quenched with increasing concentrations of AZT, as observed by fluorescence microscope (Fig. S1A–B). Subsequently, the fluorescence intensity was detected using flow cytometry, and the results showed that the fluorescence intensity gradually weakened with the concentration of AZT increased, as expected (Fig. S1C). Furthermore, to evaluate the gene editing enhancement efficiency of AZT, CRISPR-Cas9 plasmid targeting TERT gene loci was constructed, and the frequency of mutations was quantified using T7 endonuclease I (T7E1) assay, and the results indicated that the mutation frequency of TERT gene in the AZT-treated group was significantly higher than that of the other groups (Fig. S2A). The results of Western blot analysis also showed a similar trend, i.e., the lowest expression level of TERT protein was observed in the AZT treatment group (Fig. S2B), which laid a foundation for the further investigation of AZT-enhanced CRISPR-Cas9 system.

The E@M−A/RNP nanoparticles were prepared from MSN loaded with AZT, and then modified with APTES and DSP to link Cas9 RNP, followed by coated with EM as the shell (Fig. 1A). Firstly, the MSN nanoparticles with a size of about 80 nm were synthesized according to the published methods [37], and confirmed by Transmission electron microscopy (TEM), which showed a porous morphology (Fig. S3). Then, the AZT was loaded into the porous structure of MSN to obtain the MSN-AZT (M−A). The M−A was modified with (3-aminopropyl) triethoxysilane (APTES) to obtain amine groups (M−A−NH_2), and a disulfide bond containing linker [3,3-dithiodipropionic acid-di(N-succinimidyl ester), DSP] was employed to connect M−A−NH_2 and Cas9 RNP (M−A/RNP), which endowing a GSH-stimulus responsibility. Finally, the EM purified and extruded from the fresh blood and used for the outermost coating of M−A/RNP to synthesize the E@M−A/RNP nanoparticles, which were subsequently characterized by TEM, dynamic light scattering (DLS), and ζ-potential measurements. E@M−A/RNP nanoparticles appeared in spherical shape with good dispersibility under TEM observation (Fig. 1B), and the thickness of EM was estimated to be 16.0 ± 2.0 nm (Fig. S4). In the results of Fourier transform infrared (FTIR) spectrum, compared to M−A group, there was a double peak between 500–600 cm^{-1} in the M−A−DSP group, indicating the formation of disulfide bonds (Fig. S5A–B), and the characteristic peak of protein at 1636 cm^{-1} in the M−A/RNP group further indicated the successfully loading of Cas9 RNP (Fig. S5C). DLS also confirmed that the hydrodynamic diameter of MSN was 190.1 ± 2.1 nm, and that of E@M−A/RNP was 386.1 ± 6.8 nm which was 196.0 ± 4.7 nm higher than that of MSN (Fig. 1C). In addition, the changes of ζ-potential also suggested the successful modification of APTES and DSP, ligation of Cas9 RNP, and encapsulation of EM (Fig. 1D), indicating favorable synthesis of E@M−A/RNP.

The data of nitrogen adsorption indicated that the average pore size of MSN was 6.28 nm, which showed that the synthesized MSN had a large specific surface area (Fig. 1E). The highest drug loading ratio of 33.2 ± 1.4 % could be acquired until the mass ratio of MSN to AZT was close to 1: 2.5 (Fig. 1F), which suggested the high surface volume ratio of MSN. The loading efficiency of Cas9 protein was also detected using the FITC-labeled Cas9 protein, and E@M−A/RNP showed a favorable loading capacity of Cas9 protein (Fig. 1G). The ultraviolet–visible (UV–vis) data showed a broad absorption between 250 and 280 nm for M−A and E@M−A/RNP, which verified the successful encapsulation of AZT (Fig. 1H). The in vitro TME was simulated by changing the pH value and adding the glutathione (GSH), and the E@M−A/RNP nanoparticles degradation and AZT release were investigated. The results showed that AZT was released rapidly and the drug release rate could reach up to about 72.1 % (Fig. 1I). FITC-labeled Cas9 protein was used to evaluate the TME-responsive release of Cas9 RNP from the E@M−A/RNP, and

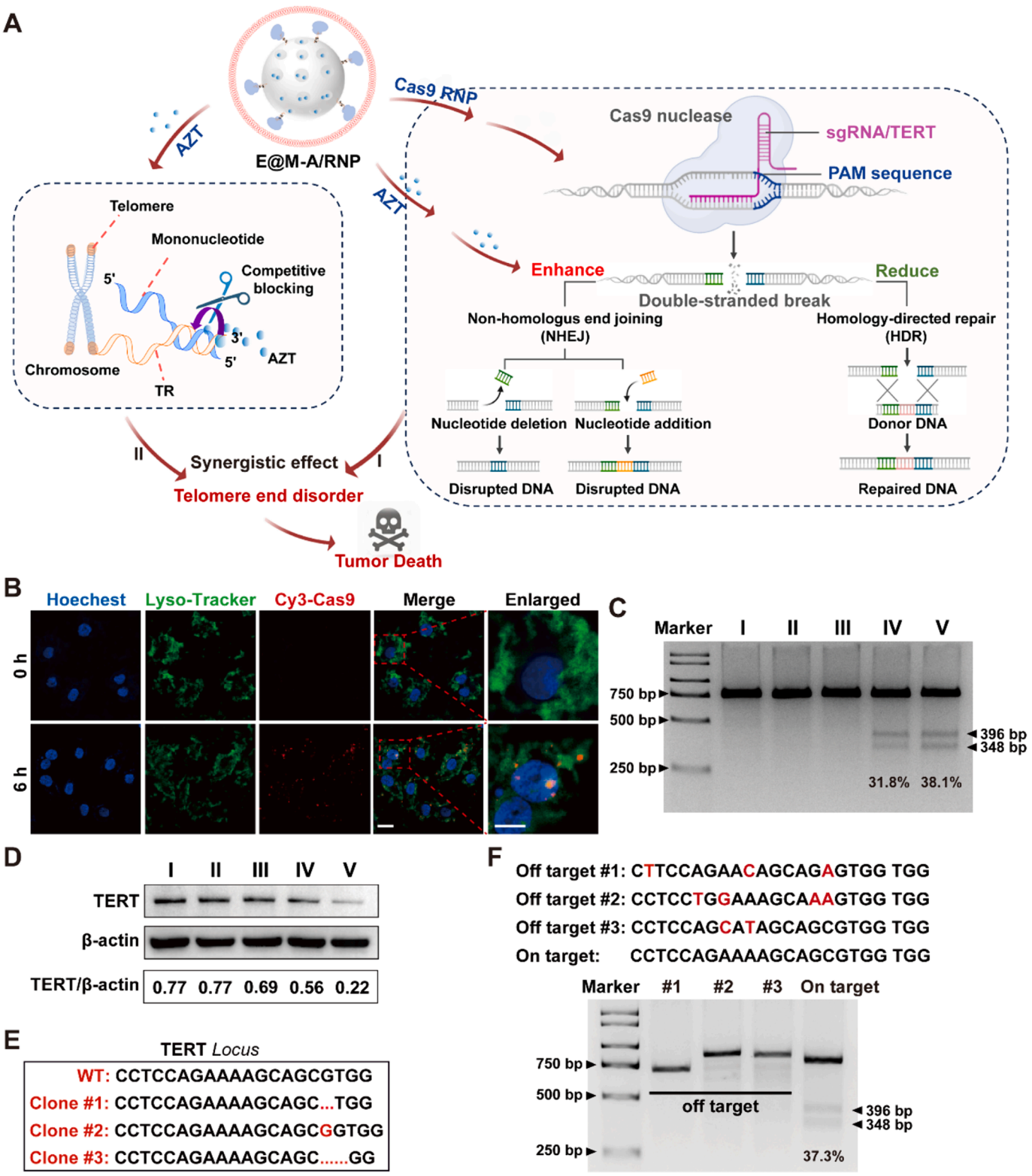

Fig. 2. Gene editing efficiency of the E@M−A/RNP nanoparticles in vitro. A) Schematic diagram of AZT regulated the frequency of Cas9 RNP gene editing by increasing NHEJ (I) and competitively inhibited the binding of single nucleotides to the telomere replication template TR (II), which leaded to telomere end disorder. B) Representative images taken by confocal laser scanning microscopy (CLSM) at different time periods (0 h, 6 h) using Cy3-labeled Cas9. Scale bar, 20 μm, enlarged scale bar, 10 μm. C) T7E1 experiment of A549 cells after different treatments. D) Western-blot analysis of protein expression of TERT. β-actin was used as a control. E) Representative DNA sequencing sequences of the TERT locus after incubation with E@M−A/RNP. F) Off-target effects detection of CRISPR-Cas9 gene editing. (I: PBS; II: E@M; III: E@M−A; IV: E@M−RNP; V: E@M−A/RNP).

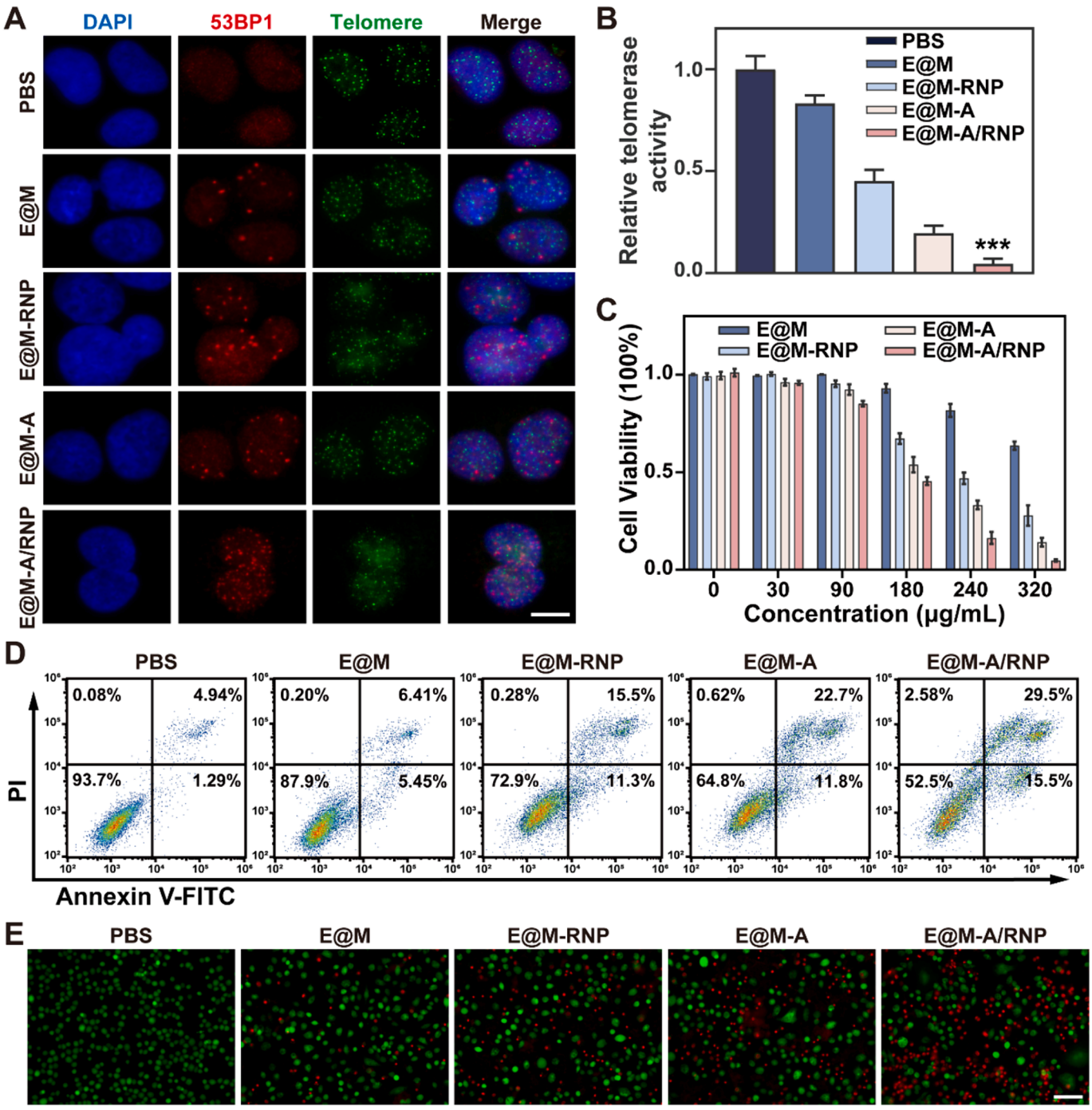

Fig. 3. Telomere end disorder induction and cell viability inhibition of the E@M−A/RNP nanoparticle in vitro. A) Telomere dysfunction inducing foci (TIF) analysis of A549 cells treated with different formulations, and performed using 53BP1 antibody (red) and TELC-FAM Probe (green) for immunostaining. Scale bar, 10 μm. B) Real-time qPCR analysis of the level of TERC in the FLAG immunoprecipitates. C) CCK-8 assays for A549 cells with different treatments. D) Flow cytometry assay for cell apoptosis studies. E) The representative fluorescent images of A549 cells with different treatments. Green, Calcein-AM (live cells) and Red, PI (dead cells). Scale bar, 100 μm. Data are shown as mean values ± S.D. (n = 3). ***$P < 0.001$. (For interpretation of the references to colour in this figure legend, the reader is referred to the web version of this article.)

the fluorescence intensity of Cas9 nuclease was enhanced with the increasing concentrations of GSH from 0 to 10 mmol/L, suggesting that the E@M−A/RNP nanoparticle successfully released Cas9 RNP in the simulated TME in vitro (Fig. S6). Furthermore, to study the integrity of EM on the E@M−A/RNP, the gel electrophoresis analysis was performed and the result indicated that the composition of membrane proteins was largely preserved and similar to that of whole blood and EM controls (Fig. 1J). The “don’t eat me” biomarker of erythrocytes, CD47, prevents RES recognition, and Western-blotting analysis confirmed that the CD47 protein was not degraded during the preparation process of E@M−A/RNP nanoparticles (Fig. 1K). These results indicated that E@M−A/RNP exhibited excellent performance in TME and showed enormous potential for tumor treatment.

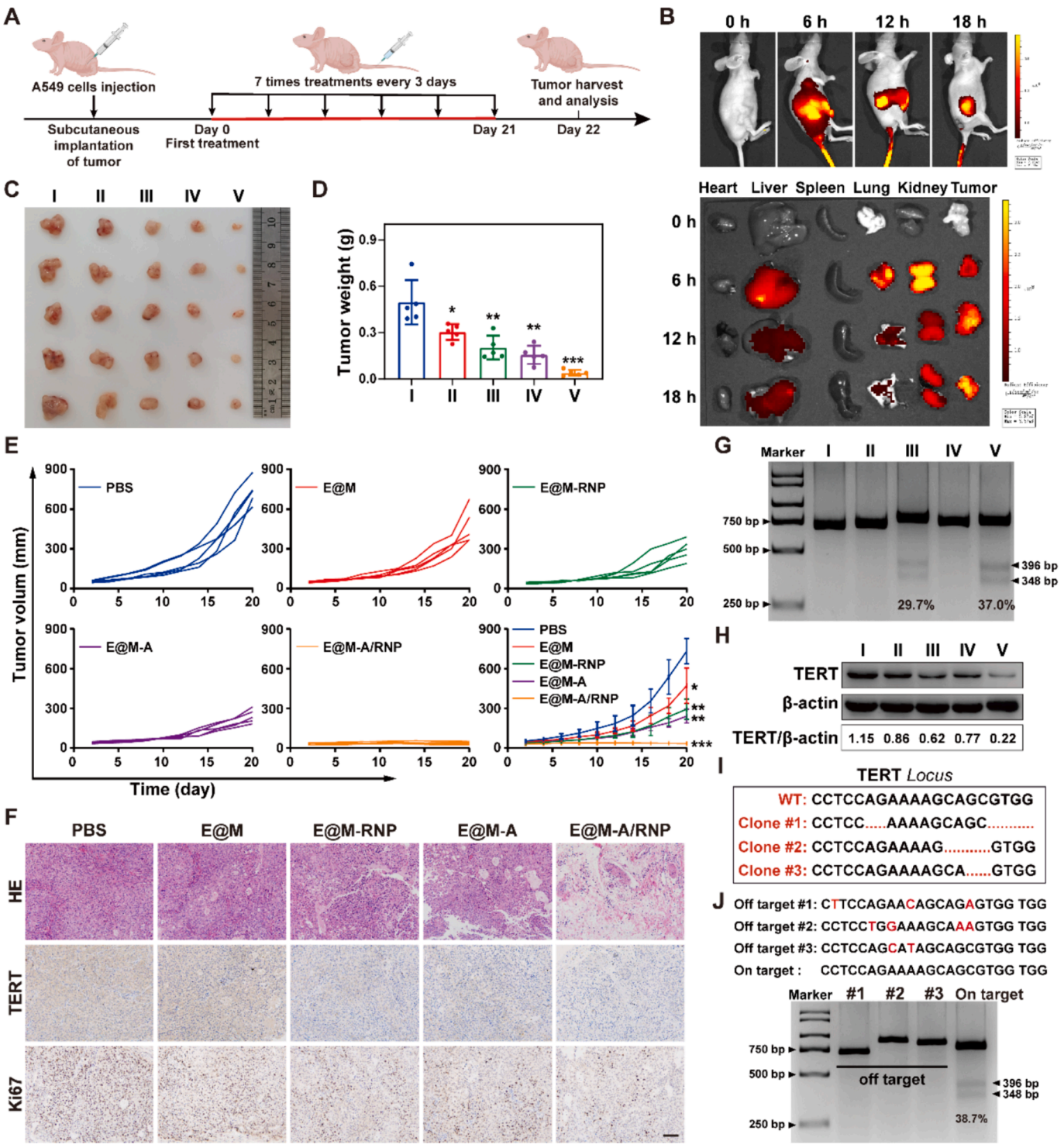

Fig. 4. Anti-tumor effects of the E@M−A/RNP nanoparticles in vivo. A) Schematic illustration of the establishment of the A549 tumor-bearing mouse model and the subsequent treatment regimen. B) Biodistribution of E@M−A/RNP nanoparticle in different major organs at 0, 6, 12, and 18 h. C) The physical photographs and D) corresponding tumor weights of the excised tumors after last administration. E) Tumor growth curves of tumors with different treatments. F) Representative H&E staining and IHC analysis of TERT and Ki67 in tumor tissues. Scale bar, 50 μm. G) T7E1 assay of tumor tissues after different treatments. H) Western-blot analysis of the protein expression of TERT in tumor tissues. β-actin was used as a control. I) Representative DNA sequencing sequences of TERT loci in tumor tissue. J) Off target effects detection of CRISPR-Cas9 gene editing in tumor tissues. I: PBS; II: E@M; III: E@M−RNP; IV: E@M−A; and V: E@M−A/RNP. Data are shown as mean values ± S.D. (n = 5). $^{*}P < 0.05$, $^{**}P < 0.01$, $^{***}P < 0.001$.

3.2. *Gene editing efficiency of the E@M−A/RNP nanoparticles in vitro*

The E@M−A/RNP nanoparticles were released both AZT and Cas9 RNP in TME, (I) AZT upregulated gene editing efficiency of Cas9 RNP by increasing NHEJ, and (II) competitively inhibited the binding of single nucleotides to the telomere replication template TR, leading to telomere end disorder (Fig. 2A). Prior to evaluation of gene editing, the internalization of E@M−A/RNP and the nuclear entry of Cas9 RNP were

confirmed. Firstly, the Cy3-labbled Cas9 protein was employed to assemble the nanoparticle, the results indicated that the significant Cy3 fluorescence signals were observed in the nucleus after 6 h of incubation, and had not yet entered the nucleus at 2 h, but a small amount of Cy3 fluorescent signal entered the nucleus at 4 h (Fig. 2B and Fig. S7), suggesting the successful lysosome escape and nuclear delivery of Cas9 RNP. The antagonistic effect of AZT on tumor cell telomeres is limited, TERT is a key gene of telomerase, and reducing the expression of TERT gene can prevent tumor cell proliferation and exert a synergistic effect with AZT. T7 Endonuclease I (T7E1) assay was performed to evaluate whether AZT enhanced the genome editing efficiency of TERT gene, and it was showed that the gene editing efficiency of the E@M−A/RNP group (38.1 %) was much higher than that of the E@M−RNP group (31.8 %) (Fig. 2C). The whole protein from treated cells were extracted for Western blot analysis. The protein expression level of TERT gene in the E@M−A/RNP treated group was significantly lower than that of the E@M−RNP and other groups (Fig. 2D). Subsequently, Small indels that were characteristic of error-prone DSB repair via NHEJ were identified at the target site by sequencing the PCR amplicons, which further confirmed the Cas9 RNP-based TERT gene editing (Fig. 2E). To verify the low off target efficiency of Cas9 RNP, the off target activates following the targeted delivery of Cas9 RNP using the E@M−A/RNP nanoparticle was evaluated, and the results showed that the extremely low off target mutation frequencies were detected (Fig. 2F). Thus, these results suggested that the E@M−A/RNP nanoparticles demonstrated an effective gene editing capability and significantly improved the efficiency of Cas9 RNP system.

3.3. The telomere end disorder induction of the E@M−A/RNP nanoparticles in vitro

AZT competitively inhibited the binding of nucleotides to the telomeric repeat amplification protocol (TRAP) template, which terminating the elongation of the telomerase DNA strand. The combination of AZT and gene editing of TERT leaded to replicative senescence in tumor cells, thereby accelerating apoptosis (Fig. 2A). Telomere dysfunction inducing foci (TIF) analysis of A549 cells treated with different material groups was performed using 53BP1 antibody (red) and TELC-FAM Probe (green) for immunostaining. After treatment of E@M−A/RNP, it was found that there were a large number of damaged proteins and the morphology of telomeres was blurred, which supported the view that cell apoptosis is caused by telomere end disorder caused by dual effects (Fig. 3A). In addition, through telomeric repeat amplification protocol (TAPR) detection, real-time PCR analysis showed a significant decrease in TERC levels in cells of the E@M−A, E@M−RNP, and E@M−A/RNP treated groups, especially in the E@M−A/RNP treated group (Fig. 3B). This may be due to the disorder of telomere terminals, which affects the total activity of telomerase and leads to changes in various components of telomeres.

To study the cell viability inhibition of E@M−A/RNP nanoparticles in tumor cells, the different concentrations of nanoparticles were treated and the Cell Counting Kit-8 (CCK-8) assay was performed. It was found that the cytotoxicity of the E@M−A/RNP treatment group was much higher than that of the other groups, and the difference in toxic effects widened with increasing concentration (Fig. 3C), where 180 μg mL^{-1} of E@M−A/RNP was close to the IC_{50} value and was selected as the concentration for subsequent therapeutic experiments. The cytotoxic effects of E@M on immortalized normal cells were also performed and the BEAS-2B and HK-2 cells were employed, it was showed that the toxic effect of E@M on normal cells was enhanced with increasing concentration, which consisted with the results of A549 cells. To be specific, the E@M exhibited negligible toxicity at concentration below 180 μg mL^{-1} and relatively high toxicity at concentration above 180 μg mL^{-1} (Fig. S8). In addition, flow cytometry analysis of cell apoptosis revealed that the apoptosis rate of E@M−A/RNP group (41.5 ± 3.1 %) was obviously higher than that of E@M−RNP (24.6 ± 2.4 %), E@M−A (33.4 ± 1.0 %), and the other groups, which consisted with the results of CCK-8 detection (Fig. 3D, and Fig. S9). The live/dead fluorescent cell staining was also performed and it was indicated a similarity result, i.e., the E@M−A/RNP treatment group showed the weakest green intensity of calcein-AM (live cells) and the highest red intensity of propidium iodide (PI, dead cells) (Fig. 3E). These above results indicated that the E@M−A/RNP nanoparticles excellently induced the telomere end disorder and thus resulting in cell viability inhibition of tumor cells.

3.4. Anti-tumor effects of the E@M−A/RNP nanoparticles in vivo

Inspired by the superior experimental results in vitro, the anti-tumor effects of the E@M−A/RNP nanoparticle was further confirmed on the A549 xenograft tumor model, which treated with different formulations via intravenous administration when the tumor volume of about 80 mm^3 (Fig. 4A). Firstly, the FITC-labeled Cas9 protein was employed to verify the biodistribution of E@M−A/RNP nanoparticles and it was found that the fluorescence signal was highly accumulation at tumor region after intravenous injection of 18 h via IVIS imaging. Subsequently, the major organs (liver, kidney, spleen, and lung) and tumor tissues were harvested after mice euthanasia, and the results indicated that the fluorescence signal in tumor tissues was gradually enhanced, and the fluorescence intensity in liver and lung organs were weakened, with the increase of time (Fig. 4B). These data suggested that the E@M−A/RNP proposed excellent tumor targeting properties, which might be due to the EM coating exerted anti-macrophage phagocytosis effect. Subsequently, A549 tumor-bearing mice were randomly divided into five groups and administrated with different formulations via intratumoral injection. The tumor volumes in all experimental groups were monitored during the next 20 days of treatment, and tumor tissues were harvested and weighed after mice euthanasia. It was observed that the tumor tissue in the E@M−A/RNP group was significantly smaller than the other groups (Fig. 4C), and the tumor weight of the E@M−A/RNP treatment group was much lighter than that of the E@M−RNP, E@M−A, E@M, and PBS treatment groups (Fig. 4D). The results of xenograft volumes in all experimental groups further confirmed the favorable tumor inhibition efficiency of E@M−A/RNP nanoparticles (Fig. 4E).

In addition, the collected tumor sections were performed for the histologic analysis. The results of hematoxylin and eosin (H&E) staining showed that the E@M−A/RNP treated group significantly reduced the cell density of tumor tissue and had a significant inhibitory effect on tumor growth (Fig. 4F). To further explore the joint strategies of drugs promoting gene editing, immunohistochemistry (IHC) staining of TERT were performed. E@M−A/RNP group exhibited the lowest expression of TERT in the tumor section, which suggested that AZT enhanced the genome editing of Cas9 RNP (Fig. 4F). IHC staining of Ki67 for cell proliferation and immunofluorescence staining of TUNEL for cell apoptosis indicated the effective anti-proliferation and pro-apoptosis effects after nanoparticles administrations, especially for E@M−A/RNP group (Fig. 4F and Fig. S10). The gene editing efficiency of E@M−A/RNP nanoparticles in tumor sections were further verified by T7E1 detection assay, and it was showed that E@M−A/RNP group (37.0 %) successfully knocked down of TERT gene and much higher than that of E@M−RNP group (29.7 %) (Fig. 4G). A similar trend was observed in the results of Western blotting, indicating that AZT and Cas9 RNP had a synergistic effect on TERT gene editing (Fig. 4H). Small insertions and deletions (indels) and off target activities were also executed in the tumor sections (Fig. 4I-J). Moreover, Q-TAPR detection showed the lowest telomerase activity in the E@M−A/RNP treated group (Fig. S11). Notably, the E@M−A/RNP nanoparticles exhibited an excellent xenograft inhibition effect and enhanced the genome editing efficiency of Cas9 RNP in vivo.

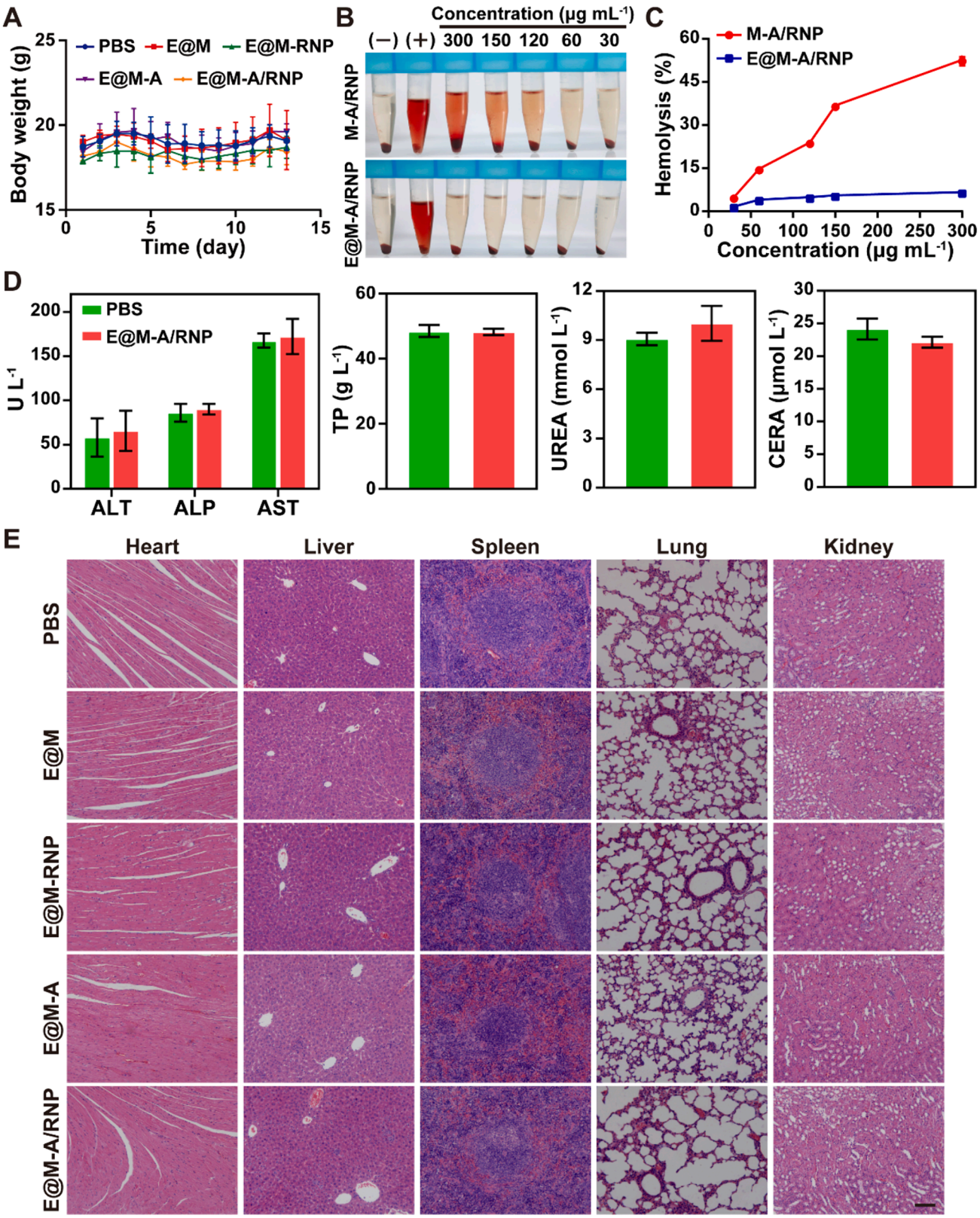

Fig. 5. Biocompatibility of the E@M−A/RNP nanoparticles. A) Body weight of mice during treatments. B, C) Assessment of hemolysis in red blood cells incubated with different concentrations of M−A/RNP and E@M−A/RNP for 6 h. D) Blood biochemical tests on the serum with treatment of PBS and E@M−A/RNP, in which alkaline phosphatase (ALP), alanine aminotransferase (ALT), aspartate aminotransferase (AST), total protein (TP), urea (UREA) and creatinine (CREA) levels were analyzed. E) H&E staining of major organs after treated with different formulations. Scale bar, 50 μm. (For interpretation of the references to colour in this figure legend, the reader is referred to the web version of this article.)

3.5. Biocompatibility of E@M−A/RNP nanoparticles

Biomembrane-camouflaged nanodelivery strategy with clinical transformation potential needs not only excellent therapeutic effects, but also highly biosafety. Thus, the biocompatibility of E@M−A/RNP nanoparticles was comprehensively evaluated. Firstly, no lethality or pronounced drop was observed in the body weight of mice after E@M−A/RNP nanoparticles treatment (Fig. 5A). Secondly, no hemolysis occurred in the E@M−A/RNP group with different concentrations after 6 h continuous exposure, while hemolysis occurred in the M−A/RNP group without EM encapsulation at low concentration (Fig. 5B-C). Additionally, extracted peripheral blood of mice from PBS and E@M−A/RNP treated groups, and serum was separated for the standard serum biochemistry detection, such as, alkaline phase (ALP), alanine aminotransferase (ALT), aspartate aminotransferase (AST), total protein (TP), urea (URA), and creatinine (CREA). The results showed that the values of these indicators were within the normal reference range (Fig. 5D). Analysis of complete blood panel tests (WBC, RBC, MCHC, MCH, HCT, MCV, Gran) showed no significant difference in all measured parameters (Fig. S12). H&E staining of the major organs' sections (heart, liver, spleen, lung, and kidney) indicated no noticeable abnormality or appreciable organ damage (Fig. 5E). All these results revealed that the E@M−A/RNP nanoparticles had high biocompatibility and favorable clinical transformation potential.

4. Conclusion

In summary, we have devised a strategy to enhance the gene editing efficacy of CRISPR-Cas9 strategy by leveraging drug synergism. Firstly, the bio-membrane camouflaged nanodelivery strategy was used and allowed for a precision delivery of CRISPR-Cas9 system to the tumor site, which maximizing its genome editing capacity and minimizing its shortcomings, such as, off-target activities. Secondly, the synergistic effect of AZT and Cas9 RNP gene editing on TERT knockdown was demonstrated and further enhanced the disruption of telomere terminals in tumor cells, thereby offering a potential anti-tumor strategy. This article establishes a biomimetic nanoplatform for delivering small molecule drugs and a CRISPR system to promote tumor cell apoptosis by enhancing telomere end disorder, E@M−A/RNP nanoparticles revealed pronounced anti-tumor synergistic therapeutic effects in both in vitro and in vivo settings. This high bio-safely nanosystem presents a novel strategy for further improving genome editing efficiency of CRISPR-Cas9 system and approach for tumor inhibition by enhancing telomere end disorder.

5. Ethics approval and consent to participate

All animal experiments were performed in accordance with the guidelines of the Committee on Experimental Animal Care and Use of Nanjing University of Chinese Medicine (approval # 202309A041) and also in accordance with the regulations of the National Ministry of Health of China.

CRediT authorship contribution statement

Silin Shi: Writing – review & editing, Writing – original draft, Methodology. **Chao Chen:** Writing – original draft. **Xueting Shen:** Methodology. **Shiyu Du:** Methodology. **Kunguo Liu:** Methodology. **Yamei Gao:** Methodology. **Lihua Qu:** Methodology. **Jingjing Yang:** Methodology. **Mengfan Tang:** Methodology. **Xin Han:** Writing – original draft.

Declaration of competing interest

The authors declare that they have no known competing financial interests or personal relationships that could have appeared to influence the work reported in this paper.

Data availability

No data was used for the research described in the article.

Acknowledgements

This work was supported by the National Natural Science Foundation of China (82302365 and 82202347), Supporting project of Nanjing University of Chinese Medicine to NSFC (XPT82202347). The Priority Academic Program Development of Jiangsu Higher Education Institutions (Integration of Chinese and Western Medicine), Jiangsu Key Discipline Construction Fund of the 14th Five-Year Plan (Biology), Natural Science Foundation of the Higher Education Institutions of Jiangsu Province, China (23KJB310015). The Graduate Research & Practice Innovation Program of Jiangsu Province (SJCX23_0845 and KYCX23_2069). The authors thank Shiyanjia Lab (www.Shiyanjia.com) for BET analysis.

Appendix A. Supplementary data

Supplementary data to this article can be found online at https://doi.org/10.1016/j.cej.2024.153152.

References

[1] H. Manghwar, K. Lindsey, X. Zhang, S. Jin, CRISPR/Cas System: Recent Advances and Future Prospects for Genome Editing, Trends Plant Sci. 24 (12) (2019) 1102–1125, https://doi.org/10.1016/j.tplants.2019.09.006.
[2] C. Chen, W. Zhong, S. Du, Y. Li, Y. Zeng, K. Liu, J. Yang, X. Guan, X. Han, Intelligent nanotherapeutic strategies for the delivery of CRISPR system, Acta Pharm. Sin. B 13 (6) (2023) 2510–2543, https://doi.org/10.1016/j.apsb.2022.12.013.
[3] S. Svitashev, C. Schwartz, B. Lenderts, J.K. Young, A. Mark Cigan, Genome editing in maize directed by CRISPR-Cas9 ribonucleoprotein complexes, Nature Communications 7 (2016) 13274, https://doi.org/10.1038/ncomms13274.
[4] F. Liu, M. Xin, H. Feng, W. Zhang, Z. Liao, T. Sheng, P. Wen, Q. Wu, T. Liang, J. Shi, R. Zhou, K. He, Z. Gu, H. Li, Cryo-shocked tumor cells deliver CRISPR-Cas9 for lung cancer regression by synthetic lethality, Sci. Adv. 10 (13) (2024) eadk8264, https://doi.org/10.1126/sciadv.adk8264.
[5] E. Chen, E. Lin-Shiao, M. Trinidad, M. Saffari Doost, D. Colognori, J.A. Doudna, Decorating chromatin for enhanced genome editing using CRISPR-Cas9, PNAS 119 (49) (2022) e2204259119, https://doi.org/10.1073/pnas.2204259119.
[6] W. Cai, T. Luo, L. Mao, M. Wang, Spatiotemporal Delivery of CRISPR/Cas9 Genome Editing Machinery Using Stimuli-Responsive Vehicles, Angewandte Chemie (International ed. in English) 60(16) (2021) 8596-8606. doi: 10.1002/anie.202005644.
[7] L. Li, S. Hu, X. Chen, Non-viral delivery systems for CRISPR/Cas9-based genome editing: Challenges and opportunities, Biomaterials 171 (2018) 207–218, https://doi.org/10.1016/j.biomaterials.2018.04.031.
[8] P. Wang, L. Zhang, W. Zheng, L. Cong, Z. Guo, Y. Xie, L. Wang, R. Tang, Q. Feng, Y. Hamada, K. Gonda, Z. Hu, X. Wu, X. Jiang, Thermo-triggered Release of CRISPR-Cas9 System by Lipid-Encapsulated Gold Nanoparticles for Tumor Therapy, Angewandte Chemie (International ed. in English) 57(6) (2018) 1491-1496. doi: 10.1002/anie.201708689.
[9] Y. Pu, H. Yin, C. Dong, H. Xiang, W. Wu, B. Zhou, D. Du, Y. Chen, H. Xu, Sono-Controllable and ROS-Sensitive CRISPR-Cas9 Genome Editing for Augmented/Synergistic Ultrasound Tumor Nanotherapy, Advanced materials (Deerfield Beach, Fla.) 33 (45) (2021) e2104641.
[10] D. Matsumoto, H. Tamamura, W. Nomura, A cell cycle-dependent CRISPR-Cas9 activation system based on an anti-CRISPR protein shows improved genome editing accuracy, Communications Biology 3 (1) (2020) 601, https://doi.org/10.1038/s42003-020-01340-2.
[11] Z. Jia, J. Choi, S. Park, Surface Charge Density-Dependent DNA Capture through Polymer Planar Nanopores, ACS Appl. Mater. Interfaces 10 (47) (2018) 40927–40937, https://doi.org/10.1021/acsami.8b14423.
[12] R.P. Barnes, M. de Rosa, S.A. Thosar, A.C. Detwiler, V. Roginskaya, B. Van Houten, M.P. Bruchez, J. Stewart-Ornstein, P.L. Opresko, Telomeric 8-oxo-guanine drives rapid premature senescence in the absence of telomere shortening, Nat. Struct. Mol. Biol. 29 (7) (2022) 639–652, https://doi.org/10.1038/s41594-022-00790-y.
[13] L. Wen, C. Zhao, J. Song, L. Ma, J. Ruan, X. Xia, Y.E. Chen, J. Zhang, P.X. Ma, J., Xu, CRISPR/Cas9-Mediated TERT Disruption in Cancer Cells, International Journal of Molecular Sciences 21 (2) (2020), https://doi.org/10.3390/ijms21020653.
[14] H. Jin, Y. Chen, J. Ren, J. Huang, Y. Zhao, H. Liu, TERC suppresses PD-L1 expression by downregulating RNA binding protein HuR, Sci. China Life Sci. 65 (12) (2022) 2505–2516, https://doi.org/10.1007/s11427-021-2085-9.

[15] H. Ebata, T.M. Loo, A. Takahashi, Telomere Maintenance and the cGAS-STING Pathway in Cancer, Cells 11 (12) (2022), https://doi.org/10.3390/cells11121958.
[16] Y. Hu, G. Shi, L. Zhang, F. Li, Y. Jiang, S. Jiang, W. Ma, Y. Zhao, Z. Songyang, J. Huang, Switch telomerase to ALT mechanism by inducing telomeric DNA damages and dysfunction of ATRX and DAXX, Sci. Rep. 6 (2016) 32280, https://doi.org/10.1038/srep32280.
[17] C.D. Richardson, G.J. Ray, N.L. Bray, J.E. Corn, Non-homologous DNA increases gene disruption efficiency by altering DNA repair outcomes, Nat. Commun. 7 (2016) 12463, https://doi.org/10.1038/ncomms12463.
[18] S.H. Rahman, S. Bobis-Wozowicz, D. Chatterjee, K. Gellhaus, K. Pars, R. Heilbronn, R. Jacobs, T. Cathomen, The nontoxic cell cycle modulator indirubin augments transduction of adeno-associated viral vectors and zinc-finger nuclease-mediated gene targeting, Hum. Gene Ther. 24 (1) (2013) 67–77, https://doi.org/10.1089/hum.2012.168.
[19] N.D. Marino, R. Pinilla-Redondo, B. Csörgő, J. Bondy-Denomy, Anti-CRISPR protein applications: natural brakes for CRISPR-Cas technologies, Nat. Methods 17 (5) (2020) 471–479, https://doi.org/10.1038/s41592-020-0771-6.
[20] D. Lim, Q. Zhou, K.J. Cox, B.K. Law, M. Lee, P. Kokkonda, V. Sreekanth, R. Pergu, S.K. Chaudhary, S.A. Gangopadhyay, B. Maji, S. Lai, Y. Amako, D.B. Thompson, H. K.K. Subramanian, M.F. Mesleh, V. Dančík, P.A. Clemons, B.K. Wagner, C.M. Woo, G.M. Church, A. Choudhary, A general approach to identify cell-permeable and synthetic anti-CRISPR small molecules, Nat. Cell Biol. 24 (12) (2022) 1766–1775, https://doi.org/10.1038/s41556-022-01005-8.
[21] W. Zhang, Y. Chen, J. Yang, J. Zhang, J. Yu, M. Wang, X. Zhao, K. Wei, X. Wan, X. Xu, Y. Jiang, J. Chen, S. Gao, Z. Mao, A high-throughput small molecule screen identifies farrerol as a potentiator of CRISPR/Cas9-mediated genome editing, eLife 9 (2020). doi: 10.7554/eLife.56008.
[22] C. Yu, Y. Liu, T. Ma, K. Liu, S. Xu, Y. Zhang, H. Liu, M. La Russa, M. Xie, S. Ding, L. S. Qi, Small molecules enhance CRISPR genome editing in pluripotent stem cells, Cell Stem Cell 16 (2) (2015) 142–147, https://doi.org/10.1016/j.stem.2015.01.003.
[23] A.M. Tejera, D.F. Alonso, D.E. Gomez, O.A. Olivero, Chronic in vitro exposure to 3'-azido-2', 3'-dideoxythymidine induces senescence and apoptosis and reduces tumorigenicity of metastatic mouse mammary tumor cells, Breast Cancer Res. Treat. 65 (2) (2001) 93–99, https://doi.org/10.1023/a:1006477730934.
[24] M.T. Mefford, J.S. Rana, K. Reynolds, O. Ranasinghe, M.A. Mittleman, J.Y. Liu, L. Qian, H. Zhou, T.N. Harrison, A.C. Geller, R.P. Sloan, E. Mostofsky, D. R. Williams, S. Sidney, Association of the 2020 US Presidential Election With Hospitalizations for Acute Cardiovascular Conditions, JAMA Netw. Open 5 (4) (2022) e228031.
[25] W. Nie, T. Yu, X. Liu, B. Wang, T. Li, Y. Wu, X. Zhou, L. Ma, Y. Lin, Z. Qian, X. Gao, Non-viral vector mediated CKb11 with folic acid modification regulates macrophage polarization and DC maturation to elicit immune response against cancer, Bioact. Mater. 6 (11) (2021) 3678–3691, https://doi.org/10.1016/j.bioactmat.2021.03.031.
[26] M. Zhang, X. Jin, M. Gao, Y. Zhang, B.Z. Tang, A self-reporting fluorescent salicylaldehyde-chlorambucil conjugate as a Type-II ICD inducer for cancer vaccines, Adv. Mater. 34 (36) (2022) e2205701.
[27] N. Qiu, G. Wang, J. Wang, Q. Zhou, M. Guo, Y. Wang, X. Hu, H. Zhou, R. Bai, M. You, Z. Zhang, C. Chen, Y. Liu, Y. Shen, Tumor-associated macrophage and tumor-cell dually transfecting polyplexes for efficient interleukin-12 cancer gene therapy, advanced materials (Deerfield Beach, Fla.) 33 (8) (2021) e2100137.
[28] S. Dong, Z. Feng, R. Ma, T. Zhang, J. Jiang, Y. Li, Y. Zhang, S. Li, X. Liu, X. Liu, H. Meng, Engineered design of a mesoporous silica nanoparticle-based nanocarrier for efficient mRNA Delivery in Vivo, Nano Lett. 23 (6) (2023) 2137–2147, https://doi.org/10.1021/acs.nanolett.2c04486.
[29] S. Wang, X. Liu, S. Chen, Z. Liu, X. Zhang, X.J. Liang, L. Li, Regulation of Ca(2+) signaling for drug-resistant breast cancer therapy with mesoporous silica nanocapsule encapsulated Doxorubicin/siRNA cocktail, ACS Nano 13 (1) (2019) 274–283, https://doi.org/10.1021/acsnano.8b05639.
[30] J. Ge, R. Tan, Q. Gao, R. Li, P. Xu, H. Song, S. Wang, Y. Wan, L. Zhou, A multifunctional nanocarrier system for highly efficient and targeted delivery of ketamine to NMDAR sites for improved treatment of depression, Adv. Healthc. Mater. 12 (21) (2023) e2300154.
[31] J. Su, H. Sun, Q. Meng, P. Zhang, Q. Yin, Y. Li, Erratum: enhanced blood suspensibility and laser-activated tumor-specific drug release of theranostic mesoporous silica nanoparticles by functionalizing with erythrocyte membranes: erratum, Theranostics 10 (5) (2020) 2401, https://doi.org/10.7150/thno.42848.
[32] X. Qin, L. Zhu, Y. Zhong, Y. Wang, G. Wu, J. Qiu, G. Wang, K. Qu, K. Zhang, W. Wu, Spontaneously Right-Side-Out-Orientated Coupling-Driven ROS-Sensitive Nanoparticles on Cell Membrane Inner Leaflet for Efficient Renovation in Vascular Endothelial Injury, Advanced science (Weinheim, Baden-Wurttemberg, Germany) 10(6) (2023) e2205093. doi: 10.1002/advs.202205093.
[33] C. Wang, X. Sun, L. Cheng, S. Yin, G. Yang, Y. Li, Z. Liu, Multifunctional theranostic red blood cells for magnetic-field-enhanced in vivo combination therapy of cancer, Advanced materials (Deerfield Beach, Fla.) 26(28) (2014) 4794-802. doi: 10.1002/adma.201400158.
[34] M. Jinek, K. Chylinski, I. Fonfara, M. Hauer, J.A. Doudna, E. Charpentier, A programmable dual-RNA-guided DNA endonuclease in adaptive bacterial immunity, Science (New York, N.Y.) 337(6096) (2012) 816-21. doi: 10.1126/science.1225829.
[35] H.A. Grunwald, A.J. Weitzel, K.L. Cooper, Applications of and considerations for using CRISPR-Cas9-mediated gene conversion systems in rodents, Nat. Protoc. 17 (1) (2022) 3–14, https://doi.org/10.1038/s41596-021-00646-7.
[36] D. Zhang, G. Wang, X. Yu, T. Wei, L. Farbiak, L.T. Johnson, A.M. Taylor, J. Xu, Y. Hong, H. Zhu, D.J. Siegwart, Enhancing CRISPR/Cas gene editing through modulating cellular mechanical properties for cancer therapy, Nat. Nanotechnol. 17 (7) (2022) 777–787, https://doi.org/10.1038/s41565-022-01122-3.
[37] L. Pan, Q. He, J. Liu, Y. Chen, M. Ma, L. Zhang, J. Shi, Nuclear-targeted drug delivery of TAT peptide-conjugated monodisperse mesoporous silica nanoparticles, J. Am. Chem. Soc. 134 (13) (2012) 5722–5725, https://doi.org/10.1021/ja211035w.